Optimization of the spatial configuration of local defects in phononic crystals for high Q cavity

Delfino Reyes[1,*], David Martínez[2], Miguel Mayorga[1], Hyeonu Heo[3], Ezekiel Walker[3,4], Arup Neogi[4,]**

[1]Faculty of Science, Autonomous University of the State of Mexico, Toluca, Mexico

[2]PhD in Science student, Faculty of Science, Autonomous University of the State of Mexico, Toluca, Mexico

[3]Echonovus Inc., Denton, TX 76205 USA

[4]Department of Physics, University of North Texas, Denton, TX 76201 USA

*** Correspondence:**
Corresponding Author
* dreyes.fc@gmail.com, ** arup@unt.edu

Keywords: Phononic crystal$_1$, waveguides$_2$, defects$_3$, Quality factor$_4$, ultrasounds$_5$.

Abstract

Defects can be introduced within a 2-D periodic lattice to realize phononic cavities or phononic crystal (PnC) waveguides at the ultrasonic frequency range. The arrangement of these defects within a PnC lattice results in the modification of the Q factor of the cavity or the waveguide. In this work, cavity defects within a PnC formed using cylindrical stainless steel scatterers in water have been modified to control the propagation and Q factor of acoustic waveguides realized through defect channels. The defects channel based waveguides within the PnC were configured horizontally, vertically, and diagonally along the direction of the propagation of the acoustic waves. Numerical simulations supported by experimental demonstration indicate that the defect-based waveguide's Q factor is improved by over 15 times for the diagonal configuration compared to the horizontal configuration. It also increases due to an increase in the scatterers' radius, which was varied from 0.7 -0.95 mm.

1 Introduction

Over the past three decades, the growing development and understanding of artificial crystal arrangements composed of periodically disposed materials with different physical properties have led to novel metamaterials. This phononic crystal and metamaterials have been utilized to control and manipulate acoustic and mechanical wave propagation (Wagner, 2016). The phononic crystal's elastic properties and the periodicity of the lattice and dimension of the scatterers produce the well-known phononic bandgaps (PnBGs). PnBGs represent the frequency ranges of the waves that are not supported within the phononic structure, and thereby their transmission through the crystal is

blocked. The PnBGs can be modified by tailoring the impedance contrast among its components, i.e., elastic constants or the mass density of the scatters and matrix, by adjusting the filling fraction ratio or the material parameters (Pennec, 2010; Zhou, 2009) or the spatial distribution of its components (Zhang Z. L., 2017; Reyes, 2019). Several manufacturing techniques have allowed the design of PnCs with tunable PnBGs through external stimulus directly acting on one or both of its components, making it possible to realize active PnCs whose acoustic properties are sensitive to electric or magnetic fields (Allein, 2016; Ponge, 2016), stress (Zhang P. J., 2017) or heat absorption (Walker E. R., 2014), among other factors. The sensitivity of materials to external stimulus has resulted in the concept of tunable PCs structures that has been proposed to manipulate acoustic wave propagation. The modification of materials properties and configuration has led to bandgap engineering and the tunable mechanical reconfiguration and materials with coupling between waveguides or defects (Wang Y. G., 2020) (Walker E. W., 2017).

PnBGs are composed of forbidden eigenmodes, which, as in solid-state theory, can be modified by inducing defects in the perfect PnC through the removal or distortion of the scatterers (Aly, 2017). Introducing a defect into the otherwise regular structure, either a point defect or a linear defect can open up small transmission windows within the PnBGs (Lucklum, 2010). It can result in an acoustic waveguide device's formation to guide waves at frequencies within the PnBG. It has been demonstrated that in a defects-based waveguide, the inter-defects separation is critical for the quality and transmissivity of the wave at the guided frequencies (Escalante, 2013) (Dong, 2017). The quality factor, $Q = f_0/\Delta f$, describes the bandwidth of a signal, were f_0 is the central frequency center of the source and Δf is the bandwidth or the full width at half maxima (FWHM) of the source. A high Q of the waveguide or cavity implies a narrow bandwidth with minimal damping and has been used as an efficient filter (Otter, 2014; Han, 2019). High-Q resonator PCs' developments essential for developing passive acoustical waveguides and modulators within integrated wireless systems and efficient acoustic signal processing systems (Han, 2019; Mohammadi, 2009). Micromechanical resonators have been used for Q factor management by tuning the external feedback control and various external pumping schemes such as optical, mechanical, thermos-piezoresistive, and parametric pumping. (Lehto Miller, 2018). The mechanical quality factor of micro- or nanomechanical resonator operating in MHz or GHz is a significant parameter to estimate the figure of merit. It is a measure of the energy decay rate in each cycle of vibrations. Q is related to the thermomechanical displacement noise, which is vital for designing force sensors and highly sensitive mechanical structures (Lehto Miller, 2018; Park, 2017). PnC-based Q-factor structures are mainly supported by inducing defect states due to broken periodicity. At the same time, in micro-resonators, it is achieved by applying an external time-varying (ac) or static (dc) energy source to the resonator (Eichler, 2011).

Phononic crystals with various Q factors have been reported and tailored mainly for operation in the high-frequency range of MHz to GHz. These structures were mostly based on micro-engineering hollowed plates (Bahr, 2014; Mohammadi, 2009). The lattice parameter of PnCs with resonance frequencies in the GHz or MHz are mostly micrometric devices with the active component of a few microns. Phononic crystals designed for low-frequency applications suffer relatively reduced scattering losses compared to GHz or MHz devices. The absolute phononic gaps in high-frequency GHz or MHz micrometric structures appear at a frequency below the Bragg limit. The localization of resonant high-frequency acoustic modes occurs in within a defect- band of the PnCs (Liu, 2000). The inclusion of tungsten in a silicon lattice yields a Q factor of 10^4 at 1.314 GHz.(Goettler, 2010). A fully planar 2D optomechanical crystal of silicon microchip consisting of a nanoscale photonic crystal cavity was shown to operate at 1.4 GHz frequency for 57 nm cavities, yielding a Q of 1.5×10^6, which strongly depends on the operating and device temperature (Mayer Alegre, 2011).

Silicon carbide PnC cavities operating in the RF and microwave showed Q factors of 2000 and 500 for 2.24 and 2.55 GHz frequency, respectively (Ziaei-Moayyed, 2011). The fabrication of high-frequency PnCs uses standard CMOS processes to realize high-Q RF MEMS resonators operating at 2.81 (Q ~ 903) and 4.54 (Q ~ 54) GHz (Bahr, 2014).

Q factors in the MHz region have also been explored. In a PnC with line defects realized by embedding a honeycomb array (lattice parameter of 15 μm) of cylindrical holes (6.5 μm) within a thin Si slab, showed Q factors of 6300 and 2128 at 126.52 MHz and 149.1 MHz, respectively (Mohammadi, 2009). A silicon PnC micromechanical resonator, manufactured by removing two rows of scattering holes from the center of the PnC was able to induce resonances in the MHz range. Q factors ranging from 1000-100 were reported in this structure (Wang N. H., 2014). A quasi-1D phononic crystal performed using dielectric membranes with a lattice parameter of ~1 mm was used to realize high Q factors, 2.2x106 and 5.2 x106 at 2.81 and 2.73 MHz, respectively (Tsaturyan, 2014). A quality factor value of 105,900 at 261.5 MHz was reported in PnC using 14.2 μm AlN unit cells with 4.7 μm air holes [24]. A Fabry-Perot SAW resonators formed between tapered PnC mirrors and patterned on a GaN-on-sapphire material platform was used to increase the Q factor at 194.07 MHz (Xu, 2018). All these reports demonstrate Q factors in the high-frequency range. However, there is not much work on optimizing the Q factor of cavities or waveguides at the low frequency. A two-dimensional PnC consisting of PZT-4D rods (175 μm) in air ambient with its lattice parameter optimized for 490 kHz was reported (Shakeri, 2019). A rod with a strain-dependent radius was introduced as a defect site within the PnC to control the defect frequency. This active phononic structure induced a resonance frequency in the kHz regime, 426.14, and 433.13 kHz, with a Q factor of around 1100. Low-frequency ultrasound in the kHz frequency range is essential for non-destructive evaluation of materials and imaging at depth.

The corresponding filtering and coupling between defects can be improved or tuned to yield Q factor optimized for different frequency intervals by adjusting the geometrical and material parameters or even the scatterers' orientation. (Wang Y. G., 2020; Lu, 2009) The coupling strength can essentially control the Q factor of PnC with defects-based waveguides. The periodicity of separation between each defect can significantly modify the Q factor when the defect is made of a scatterer with different features with respect to the rest of the defects within the PnC. (Wang Y. F., 2018; Reyes, 2019) Besides, the material and geometrical features of the defect can also influence the Q factor. In complex PnC-based Q factor structures, it can depend on the temperature, the dimensionality of the defect. (Ziaei-Moayyed, 2011)

In this work, the Q factor of a defect based waveguide is optimized. A PnC with stainless steel scatterers in water was considered with a bandgap in the kHz ranges as the basic platform for controlling acoustic wave propagation. Phononic crystals formed with varying radii of the scatterers were simulated. Acoustic waveguides were formed by defect channels that were created in a direction along and orthogonal to the direction of the propagation of the ultrasonic waves within the phononic crystal as well in a direction diagonal to the wave propagation. Results reveal that the Quality factor is enhanced by over 15 times for the diagonal configuration and is also improved by increasing the cylinders' radius while keeping constant the lattice parameter. The efficiency of the diagonal waveguide channel was corroborated using an experimental demonstration.

2 Experimental and simulation details

In order to investigate the effect of the spatial configuration of the induced defects in a perfect PnC, three PnCs with defects were considered in the COMSOL-Multiphysics platform. The perfect PnC was simulated as an array of 19×19 steel cylinders arranged as a square lattice and immersed within a water matrix. The square-shaped matrix was considered to reduce the computational effort. The cylinder diameter (d) and lattice parameter (a) were 1.6 mm and 2 mm, respectively; which yields a filling fraction of $f = \pi d^2/(4a^2) = 0.50$. The density and speed of sound were 1000 kg/m^3 and 1480 m/sec and 7800 kg/m^3 and 6300 m/sec for water and steel, correspondingly. The defects were induced by removing five cylinders in the perfect crystal, as shown in **Figure 1-A**; for each defect-line, the inter-defect distance was two periods. The yellow double arrow corresponds to a defects-line along the wave incident's direction on the crystal, i.e., for propagation along with the horizontal configuration. The green arrow denotes the vertical configuration when the defects are orthogonal to the incident wave's initial direction on the crystal. The red arrow represents the diagonal configuration. A separate figure depicts each defect line induced in a perfect PnC. The transmission spectrum was calculated from 200 to 700 kHz for the three defects-based structures and the PnC without defects.

The experimental transmission spectra of the PnCs and the different defect configurations were achieved using the ultrasonic spectroscopy technique, as shown in **Figure 1-B**. According to the above-mentioned lattice parameter and cylinder diameter, steel rods were periodically fixed capped by a bottom and top Plexiglas bases (inset in Figure 1-B, right). Two immersion transducers (*Olympus V301*) placed face to face were used as emitter and receiver (44 mm apart). The phononic structure was located between the transducers, with a distance of 2 mm of separation from either face of the transducer to avoid the near-field zone and the transducer facets' reflections. A broadband input signal from 200 to 700 kHz range was utilized from a frequency generator (*TELEDYNE Lecroy, Wave Station-2012*) to obtain each analyzed phononic structure's transmission spectrum experimentally. The output signal crossing the crystal was recorded by the other transducer that was connected to a spectrum analyzer (*Tectronix-MDO3024*) coupled to a PC for the data processing. PnC and transducers were located in a Plexiglas tank filled with 40 liters of DI water at room temperature. A picture of the defects-based structures is illustrated in **Figure 1-B** (bottom), for the horizontal, vertical, and diagonal defect configurations.

3 Results

Simulations results about the transmission features of the perfect 19×19 PnC (black line of **Figure 2**) showed two well-defined transmission bands; the first band starts at 200 kHz, and its intensity decreases at 380 kHz, while the second one is clearly identified between 480 and 580 kHz. The PnC structure provides a phononic bandgap in the range 380 < f < 480 kHz. The blue line in **Figure 2** corresponds to the transmission spectrum of the PnC for the horizontal configuration, while the green is for the vertical configuration, and the red line corresponds to the diagonal configuration, as depicted in **Figure 1-A**. It can be observed that the defects arrangement modify the bandgap in different ways. The horizontal configuration induces a new transmission band inside the bandgap from 400 kHz < f < 445 kHz, whereas the diagonal configuration has a narrow band from around 425 kHz < f < 428 kHz. It implies that the horizontal configuration opens the bandgap by around 45%, while the diagonal open it up by only 3%. The vertical defect lines do not induce strong transmission, as observed from the three peaks in the green line.

The inset plot within **Figure 2** shows the normalized transmission band induced by the defects for the horizontal and diagonal configuration with a higher resolution. For the horizontal arrangement, five resonant modes were induced; those peaks appear at 419.9, 423, 427.3, 431.5, and 434.5 kHz. The simulation of a unique defect (shown in Figure 3a) introduced in the center of the crystal showed a non-intense peak centered at 426.7 kHz, which is not present at the multi-defect horizontal. The transmission band due to the horizontal configuration is a result of the coupling of the individual resonances at each cavity-defect. For the vertical configuration (green line of Figure 2), the three small-peaks peaks in the transmission spectra were observed at 419.9, 427.3, and 434.5 kHz, which were also present in the horizontal arrangement. Interestingly, for the diagonal configuration, a narrow peak centered at 426.7 kHz was recorded. However, for this configuration, a higher resolution shows that the narrow peak is still composed of three resonances whose frequencies are 426.43, 426.68, and 426.99 kHz, and are separated by around 0.27 kHz.

Bulk bandstructure calculations of the phononic crystals having different combinations of 5 defects are presented in **Figure 3**. The whole phononic crystal was considered as the supercell, the reference primitive cell, and the primitive wave vectors of the supercell Brillouin zone were chosen to find the eigenvalues within the frequency ranging from 400 kHz to 450 kHz. The supercell bandstructure was calculated using the finite element method, COMSOL Multiphysics software. In **Figure 3**, the bandstructure for the horizontal (**3-A**) and diagonal (**3-B**) configurations shows the possible modes. The horizontal defects have five distinct modes between 420 kHz and 440 kHz, at 423.7, 427.1, 431.3, 435.7, and 438.6 kHz. In the diagonal-defect configuration, the superposition of multiple modes leads to a single dominant mode at 430.8 kHz. These modes were separated by 0.2 kHz in the transmission spectrum, with the central frequency around 430.8 kHz. (430.4, 430.6, 430.8, 431, and 432.2 kHz). The calculated eigenmodes differ by 4 kHz with respect to the transmitted peaks in **Figure 2** and occur due to the system's finite length. It should be noted that the experimentally measured transmission spectrum in **Figure 2** and the pressure maps in **Figure 4** were for the finite PnC. In contrast, the bandstructure was calculated for the infinite supercell. However, there is a qualitative agreement of the same pressure maps in **Figure 4**. The bandstructure for the perfect PnC is displayed in **Figure 3-C**. The phononic bandgap was calculated between 375 and 495 kHz, with a stopgap in the frequency interval 400-450 kHz at which the defect modes induced transmission was observed for the defect configurations. The experimentally observed transmission characteristics are well-matched with the calculated band structures and numerically calculated transmission.

From the inset in **Figure 2**, it was found that the FWHM, or simply Δf reduces from 20.66 kHz for the horizontal configuration to 1.32 kHz for the diagonal configuration, which is around sixteen times lower. Using Δf, the quality factor can be calculated as $Q = f_0/\Delta f$, where f_0 is the resonance frequency. For the horizontal (H) and diagonal (D) configurations, the quality factor is, $Q_H = 20.6$ (using the resonance peak at 427.3 kHz) and $Q_D = 323$, respectively, implying a quality factor improvement by sixteen times. This range of frequencies is particularly important for echo-sounder measurements that are performed in the zooplankton response monitoring (Churnside, 2005). It is well-known that smaller energies losses result in larger Q factors. The results show that the spatial configuration of defects can be used to control dissipation, thereby improving the Q factor of the overall acoustic waveguide. The control in the direction and intensity of propagation of ultrasonic waves can be used for pressure and temperature sensing applications. Recently the modification of the properties of cavity fluid has been used as a highly sensitive sensor platform. (Rostami-Dogolsara, 2019).

As was aforementioned, a unique defect induced in the center of the crystal, i.e., nine periods away from the emitter and receiver, breaks the symmetry and leads to a transmission peak at 426.7 kHz shown in **Figure 4-A**. Here, the pressure field of this resonant frequency is also displayed. The pressure field of all the shown frequencies was obtained from COMSOL results. By exploring within the cavity, it is observed that the energy distribution is symmetrical in both X and Y-directions. The resonance mainly occurs in the central region and is symmetrically spread out to the neighboring scatterers. **Figures 4-B** to **4-F** depict the pressure fields at five resonant frequencies for the horizontal defect configuration, which were spectrally plotted in **Figure 2**. **Figure 4-B** corresponds to the pressure field for the first resonant frequency at 419.9 kHz. The energy distribution observed in this case for the first, third, and fifth cavities shows the same energy distribution inside the cavity as observed for the single defect - the maxima energy is concentrated at the center of the cavity. However, for the second and fourth cavities, the minimum energy intensity is concentrated at the cavities center. This observed pressure distribution is produced by the periodic propagation of the guided wave. Figures 4-B to F show that each resonant frequency yields a different energy distribution at the five induced cavities. Those five resonant frequencies have a very similar wavelength between 3.46 mm and 3.40 mm. In **Figure 4-G,** the energy distribution of the diagonal configuration at 426.7 kHz is presented. The first, fourth, and fifth energy distributions are similar to the single-cavity, whereas showing an inversion in the second and third cavity. The five cavities' energy distribution is different from the observed in any other frequency of the horizontal configuration.

In **Figure 5,** the experimental results for the case simulated in **Figure 2** are displayed. There is a good agreement of the experimental results and the numerical analysis. The inset in **Figure 5** shows the expanded plot in terms of normalized power. It can be seen that the width of the transmission peak is observed for the diagonal configuration at 427.43 kHz. The experimental results showed a quality factor of $Q_H = 19.2$ (using the resonance peak at 430.26 kHz) for the horizontal arrangement and $Q_D = 255.94$ for the diagonal configuration. Shakeri and coworkers reported a Q factor of 1100 for low frequencies similar to the reported here, 426.14, and 433.13 kHz (Shakeri, 2019); however, the reported PnC consisted of microengineering PZT-4D rods of 175 μm, which requires higher and more expensive manufacturing technique than the phononic structure discussed here (steel cylinders of 0.8 mm radius).

4 Discussion

As can be seen from the previous results, the horizontal cavity configuration leads to a strong coupling between the allowed modes inside the bandgap in the presence of a defect. However, the diagonal configuration does not induce strong lateral coupling and back reflection. The decrease in the FWHM results from the tunneling of the single resonant mode, which is enhanced in the presence of the five defects. For the particular arrangement of the PnC, a defect located in the center induce asymmetry broken resonant transmission at 426.7 kHz, as was reported in **Figure 4**.

The transmission of this resonant peak is not higher in magnitude, but the bandwidth is narrower than the five-coupled horizontal defects or the weakly coupled diagonal defects due to the highest possible Q factor within the PnC structure. As shown in **Figure 2**, five-defects' combination exhibits a narrower transmission with higher intensity than a single defect (100 dBm versus 50 dBm). Experimentally, our detection system's sensitivity did not permit the observation of the transmission change due to a single defect. The five diagonally arranged defects enhance the Q factor compared to

the horizontal configuration and improve the transmitted signal's intensity compared to a single defect.

In order to help to analyze and understand the diagonal and horizontal configuration of defects, five more PnCs were numerically analyzed, keeping the lattice parameter at 2 mm, but by varying the radii as 0.70, 0.75, 0.85, 0.90, and 0.95mm, in addition to 0.80 mm which has been already described. The varying radius of the crystals results in different filling fraction $f = \pi d^2/(4a^2)$ as $f_{0.70} = 0.38$, $f_{0.75} = 0.44$, $f_{0.80} = 0.50$, $f_{0.85} = 0.56$, $f_{0.90} = 0.63$ and $f_{0.95} = 0.71$. The simulated transmission spectra of the PnCs with the varying radius of the scatters without any defects are shown in **Figure 6-A**. The PnCs with the horizontal and diagonal defect´s configurations are shown in **Figures 6-B** and **6-C**, respectively. The horizontal arrangement induces the expected five resonance peaks, while the diagonal configuration's narrow peak is also observed. For the PnC with radius 0.95 mm, an extra narrow peak was observed close to the bandgap-edge and centered at 552 kHz, for the diagonal arrangement (orange line).

The normalized power of each PnC with horizontal and diagonal configurations is shown in **Figures 7-A** and **7-B**, respectively. Here, the transmission power is presented as a staircase plot from 405 to 445 kHz. For the horizontal configuration, it is observed that the induced band is wider, and the five resonant peaks can be observed as identified by the black arrows for 0.7, 0.8, and 0.9 mm radius to exemplify the five resonant peaks. It is observed that bandwidth tends to be narrower when the radius of the cylinders increases. For the diagonal configuration, only one resonance peak is observed (each identified with the black arrow), which becomes narrower as the scatters' radius increases. For 0.95 mm, only a very narrow peak can be observed.

The numerical analysis shows that for the defects' diagonal arrangement, the quality factor is improved by over fifteen times when the radii are 0.8 mm and 35 times when it is 0.95 mm. Those results are summarized in **Figures 7-C** and **7-D**. Thus, the diagonal configuration allows a more efficient frequency-selective structure that could be used in sensing systems or wireless communication. The Q factor for the extra narrow peak recorded for the 0.95 mm radius PnC, as shown in **Figures 6-B** and **6-C**, was also calculated. It is also composed of 5 resonant peaks for the horizontal disposition while it is narrower for the diagonal configuration and centered at 552 kHz. This peak's quality factor is 136 for the horizontal and 593 for the diagonal configurations, respectively. The quality factor of the PnC with a radius of 0.95 mm was over 35 times larger for the diagonal configuration compared to the horizontal ones, 3174 vs. 89. It is well-known that the coupling strength depends on the number of scatters between each defect. If the number increases, the coupling decreases, and then, the quality factor increases. (Dong, 2017; Wang Y. F., 2018) This effect was analyzed in this revised manuscript. We conclude that it is possible to increase the quality factor by increasing the separation between defects. However, an enhancement of the Q factor values implies a loss in the transmitted signal's intensity. Additionally, it also necessitates an increased periodicity or a larger PnC. For practical applications, this fact would require a detector with higher sensitivity and a larger crystal. As the diagonal configuration does not induce strong coupling between adjacent defects, the transmission is independent of the number of defects and separation between these defects. Thus the diagonal configuration will always yield higher Q values than the horizontal defects arrangement.

The manipulation of the inner radius in hollow steel cylinders squarely immersed in water was reported (Khelif, 2003)to useful to tune the frequency and width of the guided ultrasonic signal (~170

kHz). Here, the configuration of defects induced in a perfect phononic structure and the radius of scatters shown to be crucial for Q factor and the transmitted frequency through the performed waveguide.

5 Conclusions

Numerical simulations supported by experimental demonstration indicate that the Q factor of defect based waveguides is improved by over 15 times for defects in a diagonal configuration along the propagation axis compared to their horizontal configuration, in a PnC composed of steel cylinders of 0.8 mm radius immersed in water. It also increases due to an increase in the scatterers' radius, which was varied from 0.7 -0.95 mm. For a radius of 0.95 mm, the theoretical analysis showed that the diagonal configuration's Q factor was 35 times larger than the horizontal disposition. The reason was due to the horizontal induce five defects modes with a broader induced peak. In contrast, the diagonal defects allow a single mode, due to this configuration that does not induce strong lateral coupling. Results will be useful for the high Q cavity operating in the low-frequency range using a cheap and simple PnC waveguide.

6 Conflict of Interest

The authors declare no conflict of interest.

7 Author Contributions

DR, MM, EW, and AN, performed the experimental and simulations details, besides the discussion of the results to write the manuscript, which was mainly written by DR and AN. DM performed the numerical calculations of the acoustic properties of the designed phononic structures. HH carried out the bandstructure calculations.

8 Funding

This work is supported by National Science Foundation-sponsored EFRI: NewLAW project entitled, 'GOALI: EFRI NewLaw: Non-reciprocal effects and Anderson localization of acoustic and elastic waves in periodic structures with broken P-symmetry of the unit cell' Award#1741677.

9 Acknowledgments

The authors acknowledge the above-referred funding from NSF.

10 References

Allein, F. T. (2016). Tunable magneto-granular phononic crystals. *Appl. Phys. Lett., 108*, 161903.

Aly, A. H. (2017). Phononic crystals with one-dimensional defect as sensor materials. *Indian J. Phys., 91*, 1021-1028.

Bahr, B. M. (2014). Phononic crystals for acoustic confinement in CMOS-MEMS resonators. *IEEE International Frequency Control Symposium (FCS)* (pp. 1-4). Taipei: IEEE.

Churnside, J. H. (2005). Comparison of airborne lidar measurements with 420 kHz echo-sounder measurements of zooplankton. *Applied Optics, 44*(26), 5504-5511.

Dong, H. W. (2017). Inverse design of high-Q wave filters in two-dimensional phononic crystals by topology optimization. *Ultrasonics, 76*, 109-124.

Eichler, A. C. (2011). Parametric Amplification and Self-Oscillation in a Nanotube Mechanical Resonator. *Nano Lett., 11*(7), 2699–2703.

Escalante, J. M. (2013). Dispersion relation of coupled-resonator acoustic waveguides formed by defect cavities in a phononic crystal. *J. of Physics D: Applied Physics, 46*, 1-10.

Goettler, D. S.-K. (2010). Realizing the frequency quality factor product limit in silicon via compact phononic crystal resonators. *J. of App. Phys., 108*, 084505.

Han, Y. Y. (2019). High quality factor electromagnetically induced transparency-like effect in coupled guided-mode resonant systems. *Optics Express, 27*, 7712-7718.

Khelif, A. D.-R. (2003). Two-dimensional phononic crystal with tunable narrow pass band:. *J. of App. Phys., 94*, 1308-1311.

Lehto Miller, J. M. (2018). Effective quality factor tuning mechanisms in micromechanical resonators. *App. Phys. Revs., 5*, 041307.

Liu, Z. Z. (2000). Locally resonant sonic materials. *Science, 289*(5485), 1734-1736.

Lu, M. H. (2009). Phononic crystals and acoustic metamaterials . *Materials Today, 12*(12), 34-42.

Lucklum, R. L. (2010). 1D and 2D phononic crystal sensors. *Procedia Engineering, 5*, 436-439.

Mayer Alegre, T. P.-N. (2011). Quasi-two-dimensional optomechanical crystals with a complete phononic bandgap. *Optics Express, 19*, 5658-5659.

Mohammadi, S. E. (2009). High-Q micromechanical resonators in a two-dimensional phononic crystal slab. *App. Phys. Lett., 94*, 051906.

Otter, W. J. (2014). 100 GHz ultra-high Q-factor photonic crystal resonators. *Sensors and Actuators A, 217*, 151-159.

Park, Y. R. (2017). Biotunable Nanoplasmonic Filter on Few-Layer MoS2 for Rapid and Highly Sensitive Cytokine Optoelectronic Immunosensing. *ACS Nano, 11*(6), 5697–5705.

Pennec, Y. V.-R. (2010). Two-dimensional phononic crystals: Examples and applications. *Surface Science Reports, 65*, 229-291.

Ponge, M. F. (2016). Control of elastic wave propagation in one-dimensional piezomagnetic phononic crystals. *The J. of the A. Soc. of Am., 139*, 3288.

Reyes, D. W. (2019). All-acoustic signal modulation and logic operation via defect induced cavity effects in phononic crystal coupled-resonator acoustic waveguides. *New J. Phys., 21*, 113012.

368 Rostami-Dogolsara, B. M.-F. (2019). Designing phononic crystal based tunable four-channel
369 acoustic demultiplexer. *Journal of Molecular Liquids, 281*, 100-107.

370 Shakeri, A. D.-F. (2019). Designing a tunable acoustic resonator based on defect modes, stimulated
371 by selectively biased PZT rods in a 2D phononic crystal. *Ultrasonics, 92*, 8–12.

372 Tsaturyan, Y. B. (2014). Demonstration of suppressed phonon tunneling losses in phononic bandgap
373 shielded membrane resonators for high-Q optomechanics. *Optics Express, 22*, 6810-6821.

374 Wagner, M. R. (2016). Two-dimensional phononic crystals: Disorder matters. *Nano. Lett., 16*, 5661-
375 5668.

376 Walker, E. R. (2014). Tunable ultrasonic phononic crystal controlled by infrared radiation. *Appl.*
377 *Phys. Lett., 105*, 143503.

378 Walker, E. W. (2017). Radio-frequency actuated polymer-based phononic meta-materials for control
379 of ultrasonic waves. *NPG Asia Materials, 9*, e350.

380 Wang, N. H. (2014). Evidence on simultaneous improvement of motional impedance and Q-factor of
381 silicon phononic crystal micromechanical resonators by variously engineering the cavity
382 defects. *J. of App. Phys., 115*, 094904.

383 Wang, Y. F. (2018). Channeled spectrum in the transmission of phononic crystal waveguides.
384 *Journal of Sound and Vibration, 437*, 410-421.

385 Wang, Y. G. (2020). Tunable and Active Phononic Crystals and Metamaterials. *Appl. Mech. Rev.,*
386 *72*(4), 040801.

387 Xu, Y. F. (2018). High quality factor surface Fabry-Perot cavity of acoustic waves. *Appl. Phys. Lett.,*
388 *112*, 073505.

389 Zhang, P. J. (2017). Soft phononic crystals with deformation-independent band gaps. *Proc. R. Soc. A,*
390 *473*, 20160865.

391 Zhang, Z. L. (2017). Topological design of phononic band gap crystals with sixfold symmetric
392 hexagonal lattice. *Computational Materials Science, 139*, 97-105.

393 Zhou, X. Z. (2009). Effects of material parameters on elastic band gaps of two-dimensional solid
394 phononic crystals. *J. of App. Phys., 106*, 014903.

395 Ziaei-Moayyed, M. S.-K. (2011). Silicon carbide phononic crystal cavities for micromechanical
396 resonators. *IEEE 24th International Conference on Micro Electro Mechanical Systems* (pp.
397 1377-1381). Cancún : IEEE.

398

399

400

11 Figures

Figure 1 **A**-Horizontally and diagonally local performed defects in the PnC, **B**-Experimental set up to test the transmission features; insets corresponds to the PnC (left) and the diagonal induced defect (bottom).

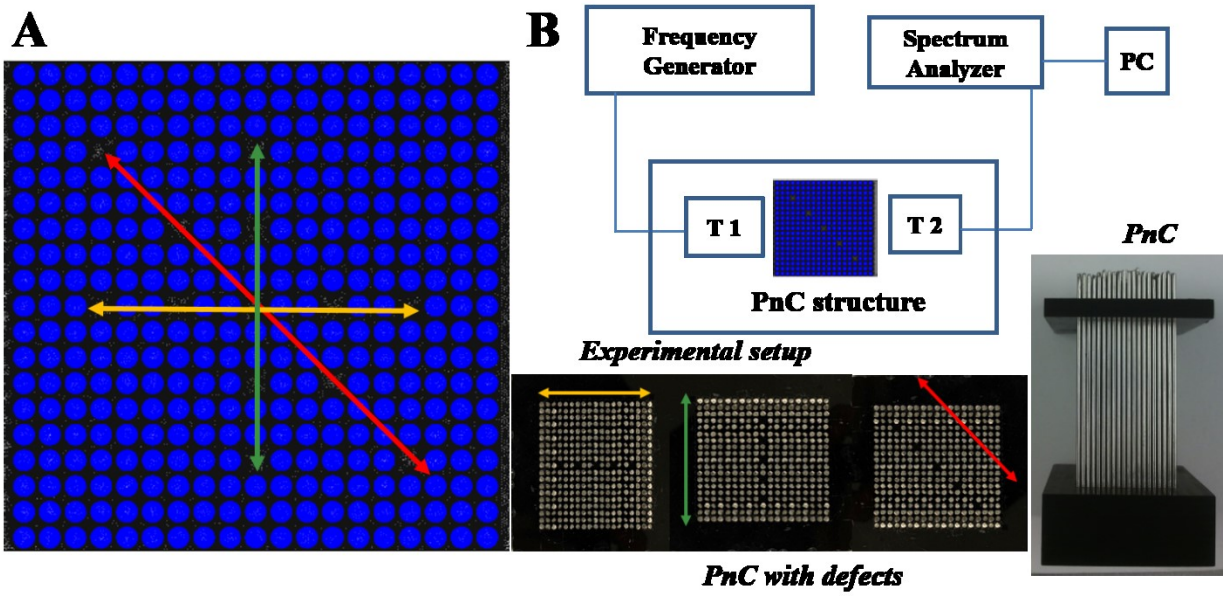

Figure 2 Theoretical transmission spectrums of the perfect PnC and the defect configurations, Inset- Normalized power for the induced band for the horizontal and diagonal configurations.

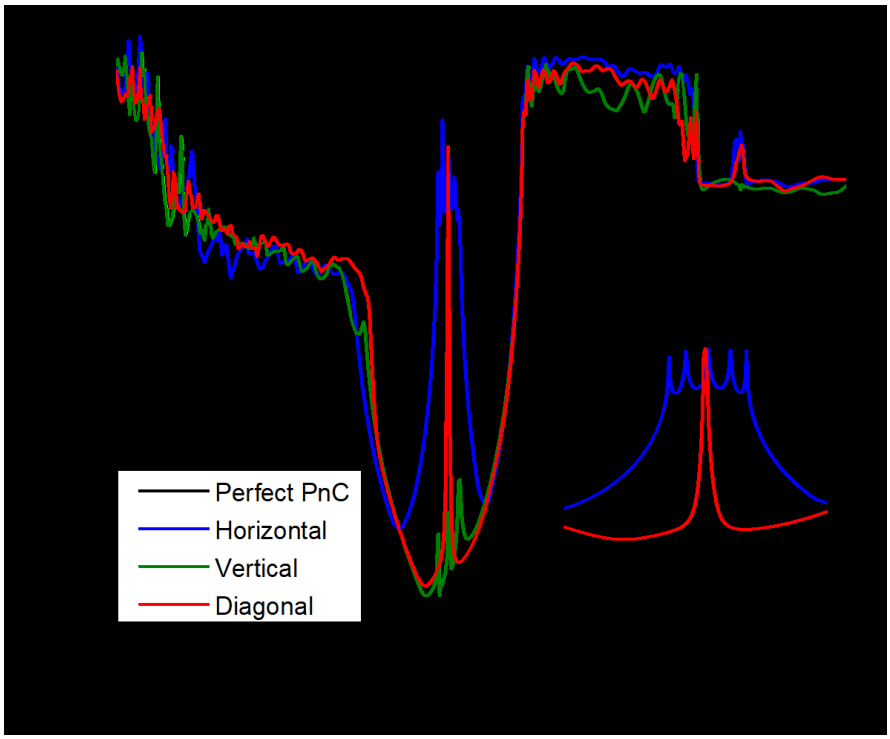

Figure 3 A-Bandstructure diagram for the horizontal configuration, **B**- Bandstructure diagram for the diagonal configuration. The inserts depict the supercell, the reference primitive cell, with 5 defects and the primitive wave vectors.

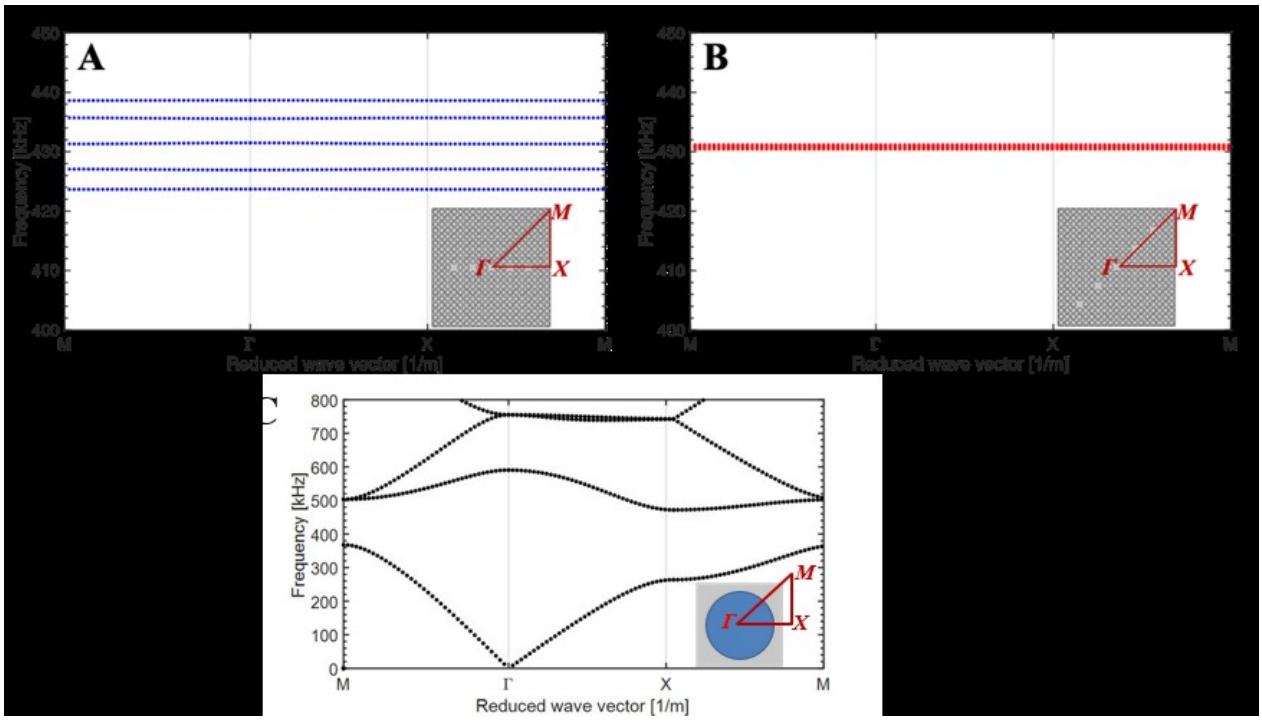

Figure 3 C-Bandstructure diagram for the perfect phononic structure.

Figure 4 A-Resonance peak and pressure map at 426.7 kHz for a unique defect induced in the center. **B** to **F**-Pressure maps for the five resonant frequencies observed for the horizontal defects configuration. **G**-Pressure map for the resonant peak at 426.7 kHz for the diagonal defects disposition.

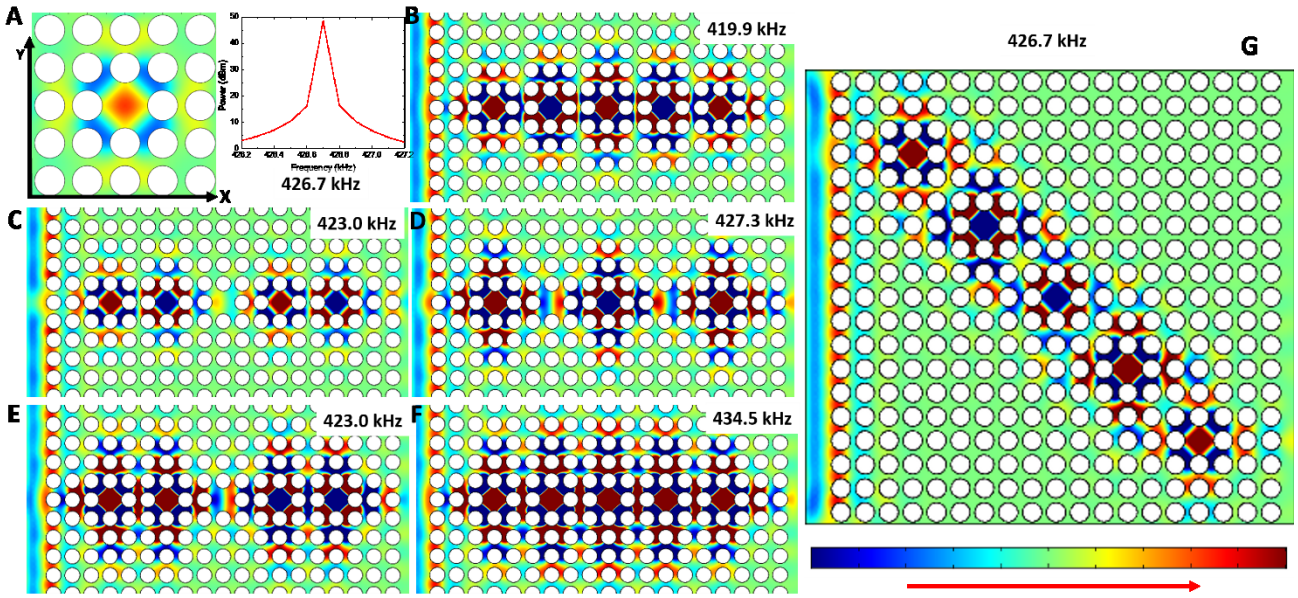

Figure 5 Experimental transmission spectrums of the perfect PnC and the defect configurations, Inset-Normalized power of the induced band for the horizontal and diagonal configurations.

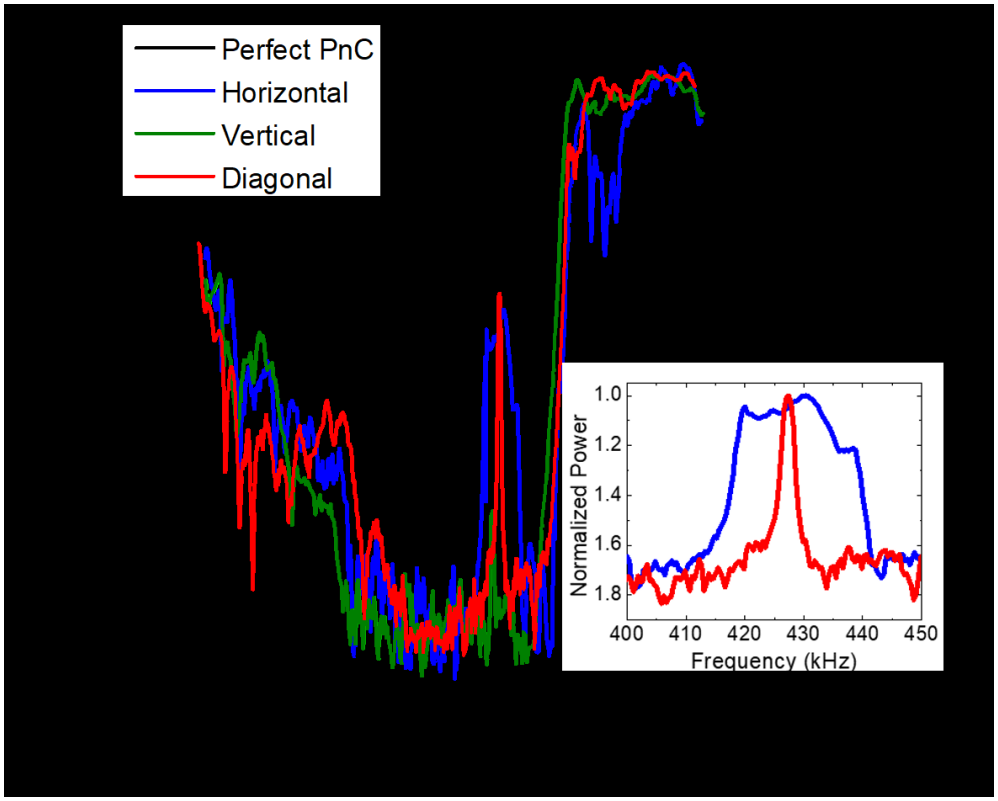

Figure 6 A-Transmission spectrums of the perfect crystal, **B**-with defects horizontally disposed and **C**-with the diagonal configuration.

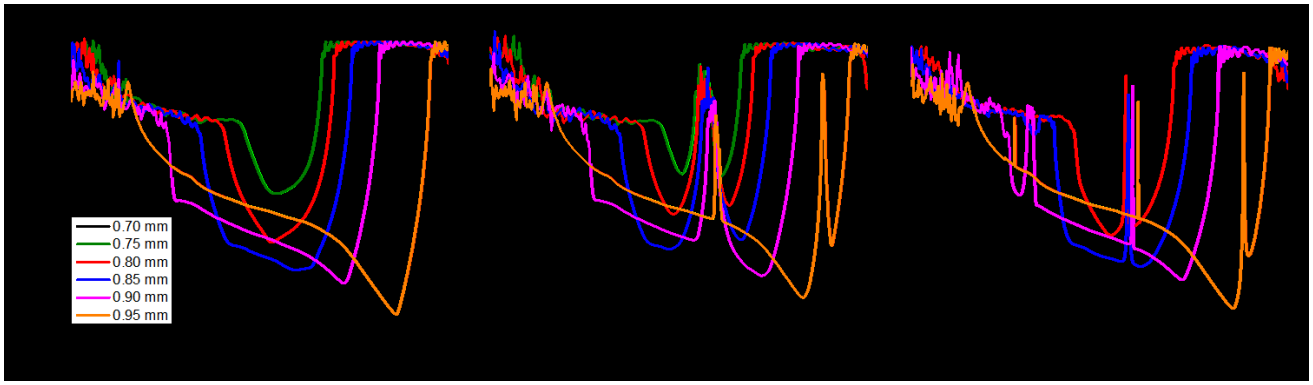

427

428

Figure 7 A-Normalized power for the horizontal disposition for the PnCs with different radius and **B**-for the diagonal configuration. **C**-Δf and **D**-Quality factor for the horizontal and diagonal configurations for the different radius.